Applied Surface Science 640 (2023) 158316

Contents lists available at ScienceDirect

Applied Surface Science

journal homepage: www.elsevier.com/locate/apsusc

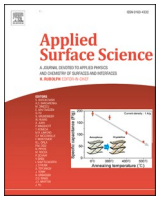

Full Length Article

Controlled electrodeposition of brookite TiO_2 for photoelectroanalysis at printed carbon electrodes

José L. Bott-Neto [a,b,*], Thiago S. Martins [a], Osvaldo N. Oliveira Jr [a], Frank Marken [b]

[a] Department of Chemistry, University of Bath, Claverton Down, Bath BA2 7AY, UK
[b] São Carlos Institute of Physics, University of São Paulo, 13560-970 São Carlos, SP, Brazil

ARTICLE INFO

Keywords:
Brookite TiO_2
Printed carbon electrodes
Electrodeposition
Vitamin C
Photoelectrochemical sensing

ABSTRACT

TiO_2-based photoelectrochemical (PEC) (bio)sensors have high photoactivity, chemical stability, and biocompatibility. However, their performance depends on multiple factors, including deposition method, morphology, and interaction with the target analyte. Herein, we describe a PEC platform based on TiO_2 electrodeposition directly onto printed carbon electrodes (without heat treatment), designed for point-of-care (POC) applications. Brookite TiO_2 nanocrystals were synthesized via electrodeposition in an acidic solution containing $TiCl_3$, and parameters such as pH and temperature were optimized to improve photoelectrocatalytic activity. Photoelectrooxidation of ascorbic acid (AA) with electrodes prepared under optimal conditions (pH 2.5, 80 °C) had 10.5 times higher photocurrents than electrodes modified with commercial TiO_2 nanoparticles via drop casting. The resulting sensor was highly sensitive and selective for AA, with a linear range from 10 to 1000 μM and a limit of detection of 3.25 μM (S/N = 3). Since brookite TiO_2 electrodeposition does not require thermal treatment, printed carbon electrodes on polymer substrates can be used in producing miniaturized devices for sensitive, selective PEC (bio)sensors.

1. Introduction

Electrochemical sensors exhibit high sensitivity and selectivity, and they are useful for clinical diagnosis and for monitoring food quality or the environment [1–5]. Photoelectrochemical (PEC) sensors, in particular, are promising for their unique ability to convert light energy into electrical signals [6]. Usually, a light pulse triggers a current associated with a local diffusional flux, which is then impeded by bio-recognition elements such as antibodies or aptamers to give the analytical signal [7–10]. The magnitude of the local photocurrent/ ion flux needs to be significant to achieve high sensor performance or sensitivity [11,12]. Improving photocurrent responses is therefore essential for a higher sensor performance. This can be reached with photoelectroactive materials such as TiO_2 semiconductor, which is used in photovoltaic devices, and photoelectrochemical sensors [13–15].

TiO_2 exhibits high photoactivity, chemical stability and biocompatibility, being found in the crystalline forms of anatase, rutile, brookite and their mixtures [16]. Anatase exhibits greater photocatalytic activity due to its slightly higher Fermi level, lower oxygen absorption capacity, and higher degree of surface hydroxylation [17]. Rutile has a narrower band gap of 3.0 eV compared to anatase, but its photocatalytic activity is one order of magnitude lower [18]. Brookite offers unique properties, such as a narrower band gap and higher charge carrier mobility, which enhance its photoelectrochemical response, making it promising for PEC sensors. However, brookite is the least studied TiO_2 polymorph due to synthesis challenges. Recent advancements in chemical techniques with post-annealing have permitted fabrication of brookite-based TiO_2 photoelectrocatalysts [13,19,20]. In particular, electrochemical deposition allows for precise control over morphology and thickness of the deposited layer [21], and efficient electrical connection to the substrate, in addition to being scalable [22,23]. It is noteworthy that electrodeposition can produce photoactive films without the need for further annealing, making it suitable for temperature-sensitive substrates such as screen-printed carbon electrodes.

In this study, we report a controlled synthesis of brookite TiO_2 crystalline phase in an anodic deposition process on printed carbon electrodes. This sensor PEC platform was characterized, and its performance was studied in detecting ascorbic acid as a proof- of-concept analyte. A 10.5-fold increase in photocurrent was obtained for electrodes prepared via electrodeposition compared to electrodes modified

* Corresponding author.
E-mail address: joseluiz.bott@gmail.com (J.L. Bott-Neto).

https://doi.org/10.1016/j.apsusc.2023.158316
Received 19 May 2023; Received in revised form 2 August 2023; Accepted 22 August 2023
Available online 25 August 2023
0169-4332/© 2023 The Author(s). Published by Elsevier B.V. This is an open access article under the CC BY license (http://creativecommons.org/licenses/by/4.0/).

via drop casting TiO_2, with a resulting sensing performance considerably higher than those reported in the literature [15]. The higher photoelectrocatalytic performance was attributed to a better coating of the conductive surface and an improved contact between TiO_2 film and the carbon substrate. The main novelty in the work is therefore in the use of electrodeposited brookite TiO_2 without thermal annealing. This allows for sensors on printed electrodes since no thermal treatment is required, thus favoring miniaturization of PEC devices.

2. Experimental

2.1. Reagents

Titanium (III) chloride solution 20% (w/v), hydrochloric acid (HCl), potassium chloride (KCl), sodium bicarbonate ($NaHCO_3$), sodium chloride (NaCl), sodium phosphate dibasic (Na_2HPO_4), potassium phosphate monobasic (KH_2PO_4), potassium hexacyanoferrate (II) trihydrate ($K_4[Fe(CN)_6].3H_2O$), and potassium hexacyanoferrate (III) ($K_3[Fe(CN)_6]$), titanium oxide power (TiO_2; nanopowder, less than25 nm particle size, Anatase, Product Number: 637254) were obtained from Sigma-Aldrich. The Ag/AgCl conductive ink used on the reference electrode was obtained from TICON® (Sorocaba, Brazil). Ultrapure water provided by a Thermo Fisher system had 18.2 MΩ cm resistivity. Phosphate buffer saline (PBS) solution at pH 7.4 was prepared with 137 mmol/L NaCl, 2.7 mmol/L KCl, 10 mmol/L Na_2HPO_4, and 1.8 mmol/L KH_2PO_4. In addition, a 5 mM $Fe(CN_6)^{3-/4-}$ solution was prepared in 0.1 M KCl, which contained 5 mM $K_4[Fe(CN)_6]$ and 5 mM $K_3[Fe(CN)_6]$.

2.2. Apparatus

Scanning electron microscopy (SEM) images were recorded at a 5.0 kV accelerating voltage with a JOEL JSM-7900F instrument, which also allowed for energy-dispersive X-ray spectroscopy (EDX, Ultim Max 170 mm^2). Raman analyses were performed using the Renishaw Qontor confocal Raman microscope with an excitation wavelength of 532 nm. Electrochemical impedance spectroscopy (EIS) experiments were recorded with a CompactStat (Ivium Technologies, Netherlands), while the other electrochemical experiments were performed with a Metrohm Autolab potentiostat (PGSTAT12).

2.3. Electrodeposition of TiO_2 on SPCE

Screen-printed carbon electrodes (SPCEs) were fabricated on polyethylene terephthalate (PET) substrates, as described previously [2]. Before electrodeposition, the SPCEs underwent an electrochemical treatment involving two cycles of potential cycling between −3.0 V and + 2.5 V versus a pseudo-reference carbon electrode at 100 mV s^{-1}. Then, amorphous or crystalline titanium dioxide (TiO_2) was electrodeposited onto the SPCEs according to a literature procedure [24]. To electrodeposit TiO_2, a conventional three-electrode cell with temperature control was employed (Scheme 1). The platinum mesh and silver/silver chloride electrode (Ag/AgCl, saturated KCl) were used as auxiliary and reference electrodes, respectively. Electrodeposition of TiO_2 was carried out in a $TiCl_3$ solution (25 mM). The solution was saturated with nitrogen and

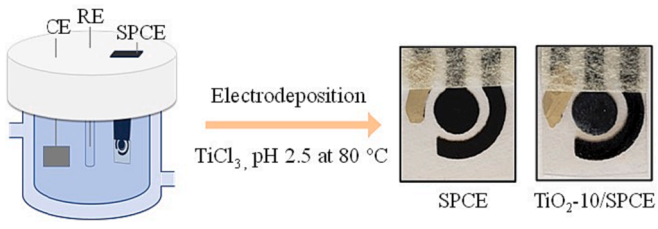

Scheme 1. (i) Electrochemical cell with temperature control. (ii) SPCE before and after electrodeposition of TiO_2 for 10 min.

the pH adjusted to 2.0, 2.5 or 3.0 using $NaHCO_3$ solution. A potential of 1.5 V (vs. Ag/AgCl, saturated KCl) was applied for 5, 10, 30 and 60 min, at temperatures of 60 °C and 80 °C. The electrodes prepared for 5, 10, 30 and 60 min at 80 °C are referred to here as TiO_2-5, TiO_2-10, TiO_2-30, TiO_2-60, respectively. After electrodeposition, the electrodes were dried at room temperature, and one of the carbon electrodes was painted with silver/silver chloride paint to be used as a pseudo reference electrode ($Ag/AgCl_{pseu}$). Furthermore, to prepare electrodes with TiO_2 nanoparticles via drop casting, 6 μL of TiO_2 (1 mg mL^{-1}) was applied to the electrode surface using optimized conditions under [15], and subsequently dried under vacuum at room temperature. Additionally, previous studies have provided details regarding the characterization of the used commercial TiO_2, revealing that the material primarily comprises nanoparticles, predominantly in the anatase phase, with an average crystalline size of 20 nm [15].

2.4. Analytical procedure

Ascorbic acid (AA) solutions were prepared by dissolving AA in PBS solution, at concentrations ranging from 1 to 1000 μM. The analytical curves were obtained by recording the photocurrent generated by AA solutions at the TiO_2-based working electrode after 132 s illumination (410 nm, 350 mW cm^{-2}). A potential at 0 V was applied vs open circuit potential (OCP), which was predetermined for 120 s and equal to −0.08 V vs Ag/AgCl. The analytical curves for photocurrent versus AA concentration were fitted using linear regression analysis and the limits of detection (LOD) and quantification (LOQ) were calculated using the least square regression method [25].

3. Results and discussion

3.1. TiO_2 electrosynthesis optimization

Fig. 1**a** shows transient photocurrent curves for 0.1 M AA in PBS solution for electrodes prepared at pH 2.0, 2.5, and 3.0 at 60 and 80 °C for 30 min. The photocurrents for electrodes prepared at 60 °C and pH 2.0, 2.5 and 3.0 were 0.3, 1.0, and 1.3 μA, respectively. In contrast, the photoelectrocatalytic activity of electrodes prepared at 80 °C is significantly higher, with photocurrents of 6.7, 9.9, and 5.8 μA for modified electrodes at pH 2.0, 2.5, and 3.0, respectively. The effect of electrodeposition time for the modified electrodes at 80 °C and pH 2.5 is shown in Fig. 1**b**. The photocurrent increases for electrodes prepared between 5 and 10 min, but it decreases for those synthesized from 10 to 60 min. For the latter electrodes the current takes longer to stabilize. These findings provide important insights into the factors determining the photocurrent response of TiO_2 over printed electrodes and highlight the potential of adjusting preparation conditions to optimize performance. As shown in Fig. 1**b**, the TiO_2-10 electrode has a photocurrent of ca. 10 μA, which represents a 10.5 fold increase compared to electrodes with drop cast nanoparticles (TiO_2 NPs). In part, this better performance can be attributed to improved electrical contacts created by the electrodeposition methodology.

3.2. Electrochemical characterization

To investigate the electrochemical properties of TiO_2 electrodes, EIS and CV measurements were conducted in 5 mM $[Fe(CN)_6]^{3-/4-}$ in 0.1 M KCl. The Nyquist plots in Fig. 1**c** indicate an increase in charge transfer resistance for modified electrodes compared to bare SPCE. This resistive behavior is attributed to TiO_2 accumulation on the SPCE, which prevents direct charge transfer of $[Fe(CN)_6]^{3-/4-}$ complexes. Using the circuit in **Fig. S1** to fit the data, the estimated charge transfer resistance for SPCE, TiO_2 NPs, and TiO_2-10 are 4.3, 8.9, and 34 kΩ. The cyclic voltammograms obtained under the same conditions in Fig. 1**d** corroborate the EIS results. The modified SPCE via drop casting exhibits a similar profile to the unmodified SPCE, and the current arising from the $Fe^{(II)}/Fe^{(III)}$ redox

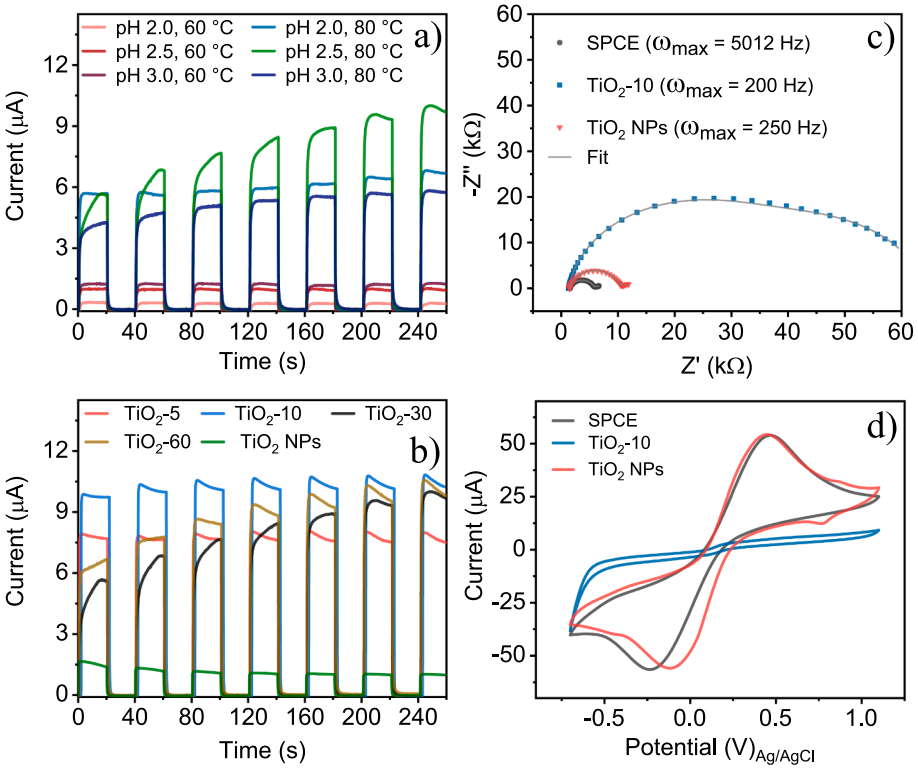

Fig. 1. Transient photocurrent curves were obtained under the following conditions: (a) TiO_2 electrodeposited for 30 min at different pHs (2.0, 2.5, and 3.0) and temperatures (60 °C and 80 °C); (b) TiO_2 electrodeposited at pH 2.5 and 80 °C for different deposition times: 5 min (TiO_2-5), 10 min (TiO_2-10), 30 min (TiO_2-30), and 60 min (TiO2-60), and TiO2 nanoparticle electrodes prepared using drop casting (TiO2 NPs). The measurements (pictures a and b) were recorded in PBS containing 0.1 M AA at 0 V (vs. OCP) under 410 nm irradiation. (c) EIS spectra (frequency range from 1 Hz to 10 kHz; bias 0 V vs OCP; 10 mV amplitude;) and (d) cyclic voltammograms at 50 mV s^{-1} of SPCE, TiO_2-10, and TiO_2 NPs in 0.1 M KCl containing 5 mM $[Fe(CN)_6]^{3-/4}$.

couple for the TiO_2-10 electrode is very small. The drop casting method produces discontinuous films prone to unwanted back reactions (substrate recombination) in photoelectrochemical processes [26]. Electrodeposited TiO_2 electrodes had a lower current for $Fe^{(II)}/Fe^{(III)}$ redox processes, while the electrode modified via drop casting exhibited a voltammetric profile similar to bare SPCE. This means that a considerable portion of the electrode is exposed to allow for back reduction to occur, which could explain the lower photocurrents for TiO_2 modified via drop casting compared to electrodeposited electrodes.

3.3. Structure and morphology

Fig. 2**a** shows Raman spectra of electrodeposited TiO_2 under different conditions, recorded with 3 mW, which is sufficiently low to avoid structural changes to the materials [27]. For the electrode prepared during 60 min, an intense vibration mode appears at 153 cm^{-1} assigned to the A_{1g} mode, characteristic of the brookite phase. The weak signals at 252 (A_{1g},), 322 (B_{3g},), 412 (A_{1g}), and 633 cm^{-1} (A_{1g}) [27–29] confirm the presence of the brookite phase. The Raman spectra for TiO_2-30 and TiO_2-10 electrodes have a similar profile. However, for the electrodes prepared for 5 min at 80 °C and 30 min at 60 °C in **Fig. S2**, the Raman signals are very weak due to the low amount of TiO_2 on the carbon substrate. Additionally, the Raman spectrum of commercial TiO_2 NPs exhibit bands at 144 (E_g), 396 (B_{1g}), 516 (B_{1g}) 638 cm^{-1}(E_g), which are typically attributed to the anatase phase (Fig. 2**a**) [30]. The HR-TEM image in Fig. 2**b** displays a d = 0.35 nm lattice spacing that can be assigned to (110) or (210) planes of anatase or brookite phases, respectively [31]. Fig. 2**c** shows the electron diffraction patterns for the same electrode, and the spacing values obtained are listed in **Table S1**. The D-spacings 3.541, 2.976, 2.399, and 1.900 Å are attributed to (210), (211), (012), (321), and (421) planes of the brookite TiO_2 structure, respectively.

SEM images of TiO_2-based electrodes were analyzed to investigate their morphology and surface density. The image for SPCE before modification in Fig. 3**a** is typical of a rough surface of amorphous carbon (carbon black) and graphite. The SEM images for modified electrodes at 60 and 80 °C for 30 min show increased film density for electrodeposited electrodes at the higher temperature, according to Fig. 3**b** and Fig. 3**e**.

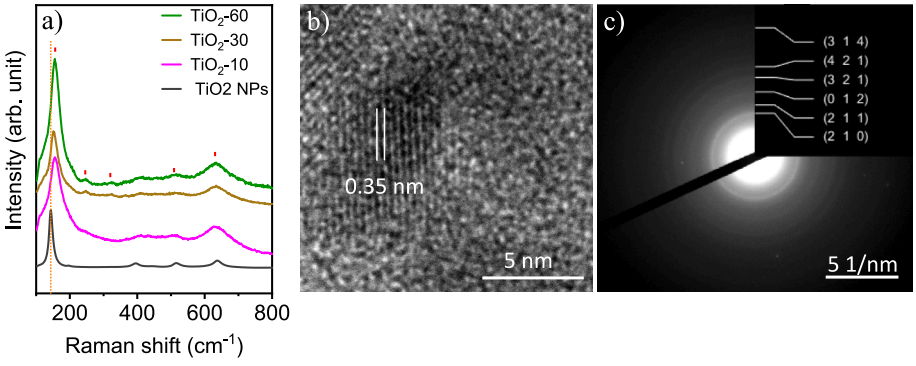

Fig. 2. (a) Raman spectra of commercial TiO_2 NPs and TiO_2 electrodeposited for 10 (TiO_2-10), 30 (TiO_2-30), and 60 (TiO_2-60) min at pH 2.5 and 80 °C. (b) HR-TEM image and (c) electron diffraction of TiO_2 electrodeposited at 80 °C for 10 min (TiO_2-10).

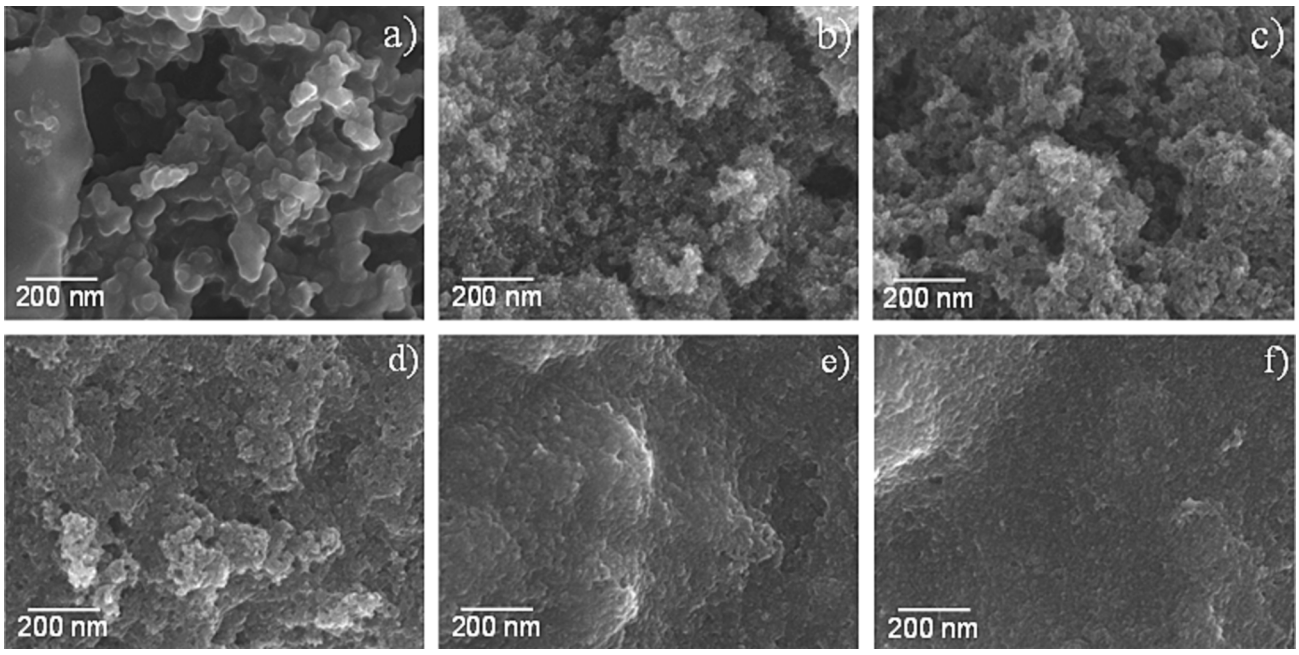

Fig. 3. SEM images of the electrodes at 100 k times magnification: (a) SPCE, (b) TiO_2 electrodeposited at 60 °C for 30 min, (c), TiO_2-5, (d) TiO_2-10, (e) TiO_2-30, and (f) TiO_2-60.

More compact, homogeneous structures were obtained in Fig. 3**c-f** by increasing electrodeposition time between 5 and 60 min at 80 °C. **Fig. S3** displays lower-magnification SEM images. Several cracks are observed throughout the film. The presence of microcracks in electrodeposited films is not uncommon and can occur in various electrodeposition methods. However, it is worth noting that the presence of microcracks does not necessarily invalidate the deposited film. In fact, in certain cases, microcracks can even be desirable, especially in applications such as sensors, where a larger surface area is beneficial. The cross-sectional images in Fig. 4**a-b** and **Fig. S4** reveal a 1.7 ± 0.7 μm thick film for the electrode prepared at 10 min, 80 °C, and pH 2.5. The EDX analyses of different areas depicted in Fig. 4**c-f** and **Fig. S5** indicate a homogeneous distribution of titanium on the surface of the SPCE electrode.

3.4. Analysis of PEC sensor performance for ascorbic acid

Fig. 5**a** shows the transient current curves for different AA concentrations, which can be described by equations 1 through 4. In the absence of AA, the photocurrent arises from oxidation and reduction reactions of water and oxygen, described by equations 2 and 3, respectively. For concentrations above 10 μM, the photocurrent increases linearly with AA concentration up to 1000 μM according to the equation $I/nA = 0.1137\ C_{AA}/\mu M + 27.46$ ($r^2 = 0.994$, N = 3), where C_{AA} is the AA concentration, and I is the photocurrent intensity at 132 s. This suggests that AA oxidation is the prevailing process. The limit of detection (LOD) value was estimated as 3.25 μM (S/N = 3).

$$TiO_2 + h\nu \rightarrow e^- + h^+ \quad (1)$$

$$O_2 + e^- \rightarrow {}^{\bullet}O_2^- \quad (2)$$

$$H_2O + h^+ \rightarrow {}^{\bullet}OH \quad (3)$$

$${}^{\bullet}O_2^-/{\bullet}OH/h^+ + AA \rightarrow AA^+ \quad (4)$$

The performance of our PEC sensor using brookite TiO_2 on SPCE for AA detection exhibited promising results compared to previous studies, as shown in Table 1. These findings highlight the potential of our approach for accurate and efficient AA detection in various applications. The selectivity of the PEC sensor towards the target analyte was assessed with experiments in the presence of potential interferents, namely uric acid, lactate, dopamine, glucose, sodium chloride, and potassium chloride. Fig. 5**c** confirms the high degree of selectivity without effects from the tested interferents. The stability and reproducibility of the PEC sensor were evaluated through measurements to detect 500 μM AA, whose results in Fig. 5**d** demonstrate the reproducibility with a relative standard deviation (RSD) of 3.9% in photocurrent measurements taken using 6 distinct electrodes. In the stability tests, the photocurrent was recorded under irradiation during 20 s on/off cycles, and the standard deviation was 0.95%. These findings suggest that the PEC sensor is reliable and can produce consistent results. Recovery measurements were performed with Vitamin C tablet in PBS solution using the standard addition method. The AA concentrations calculated from the analytical curve and other parameters are summarized in **Table S2**. Recovery for the PEC sensor ranged between 95.0% and 98.7%, with relative standard deviation (RSD) less than 4.1%. These satisfactory results confirm the potential application in pharmaceutical analysis.

3.5. Implications

The TiO_2-10 PEC sensing platform is not limited to the direct detection of ascorbic acid. It may also be employed in PEC biosensors where AA acts as a redox probe to yield signal amplification. For example, the electrode can be modified with recognition biomolecules such as oligonucleotides and antibodies for detecting non-electroactive biomarkers. Under light irradiation, the photogenerated charge carriers interact with AA, which acts as an electron donor, thus increasing the photocurrent generated [15]. In general, concentrations between 0.1 and 0.2 M AA are used in PEC biosensors [1,15,40–42]. The intensity of photogenerated current is highly dependent on the interaction of AA with the semiconductor surface. Therefore, any changes in the film resulting from an immunoreaction can affect the photocurrent signal. If the concentration of biomolecules is high, the AA flux is impaired and the photocurrent decreases. The biosensor would then operate by signal suppression.

4. Conclusion

This study has shown that the controlled electrodeposition of

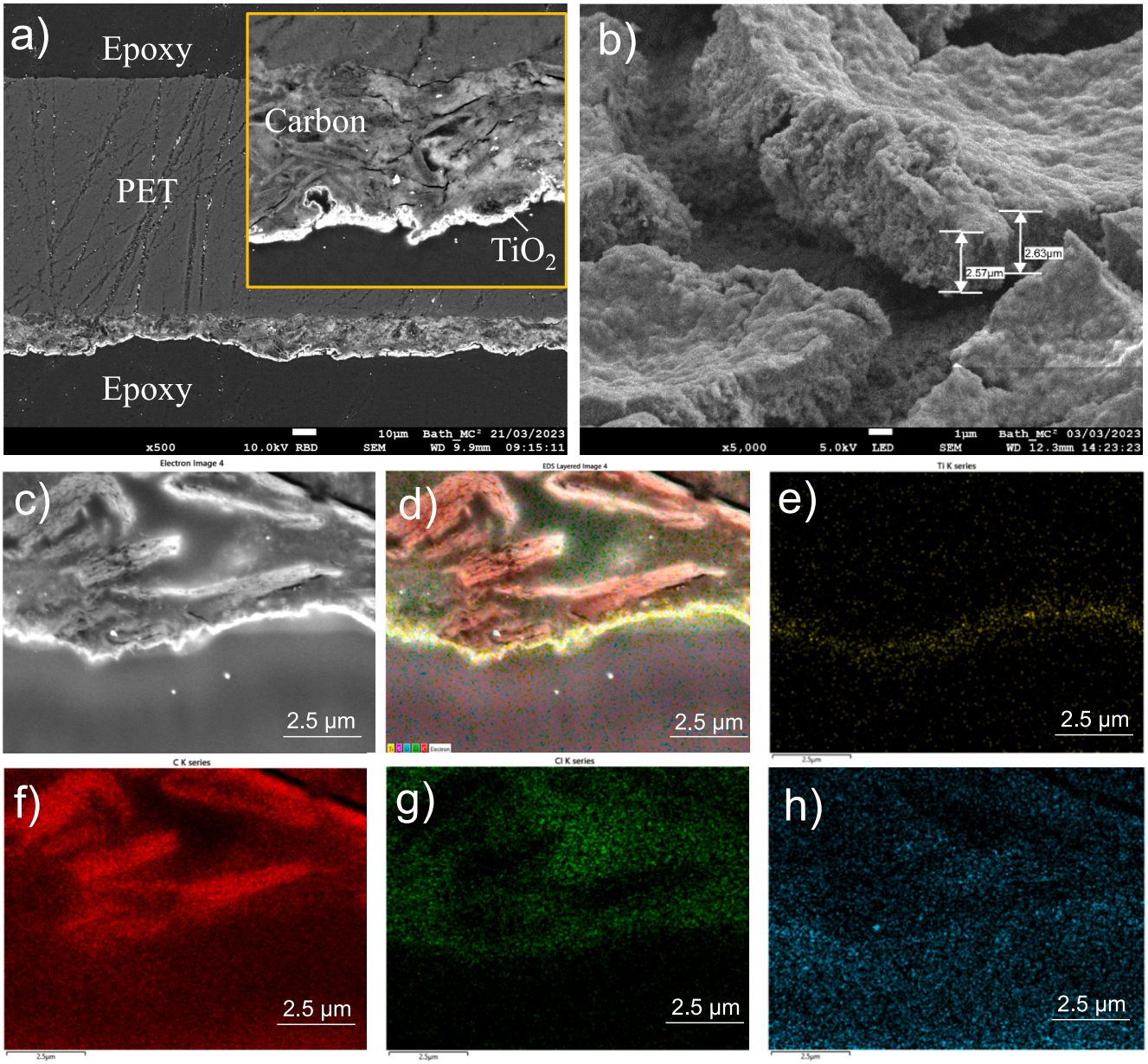

Fig. 4. (a-b) Cross-section SEM image of TiO_2 electrodeposited for 10 min at pH 2.5 at 80 °C. EDS analysis: (c) electron image, (d) EDS layered image, (e) Ti K, (f) C K, (g) Cl K, (h) O K series.

brookite TiO_2 on printed carbon electrodes is effective, holding promise for a TiO_2-based photoelectrochemical detection platform. The TiO_2 film on carbon was photochemically active without thermal annealing, which could be (at least in part) linked to the electrodeposition process creating good electrical contacts to the substrate. However, further study will be required to reveal further physico-chemical aspects (effects of crystal structure, morphology and grain boundaries, light absorption, charge mobility, recombination, etc.) and to further improve performance. This platform ability to operate under visible LED light irradiation makes it versatile and applicable to various biosensor scenarios, since ultra-violet light can be harmful to biomolecules. The brookite phase of TiO_2 shows superior photoelectrocatalytic activity for oxidation of ascorbic acid compared to drop casting of commercial TiO_2 nanoparticles. The optimal conditions for electrodeposition were found to be pH 2.5 and 80 °C. The method of TiO_2 fabrication over porous carbon electrodes can be explored for other applications such as printed photovoltaic and photoelectrochemical pollution treatment systems. Overall, this work highlights the importance of electrodeposition to create well-connected semiconductor films on carbon substrates and the benefits of obtaining the brookite phase of TiO_2.

CRediT authorship contribution statement

José L. Bott-Neto: Investigation, Conceptualization, Methodology, Writing – original draft, Writing – review & editing. **Thiago S. Martins:** Conceptualization, Methodology, Writing - review & editing. **Osvaldo N. Oliveira Jr:** Funding acquisition, Supervision, Writing – review & editing. **Frank Marken:** Funding acquisition, Supervision, Writing – review & editing.

Declaration of Competing Interest

The authors declare that they have no known competing financial interests or personal relationships that could have appeared to influence the work reported in this paper.

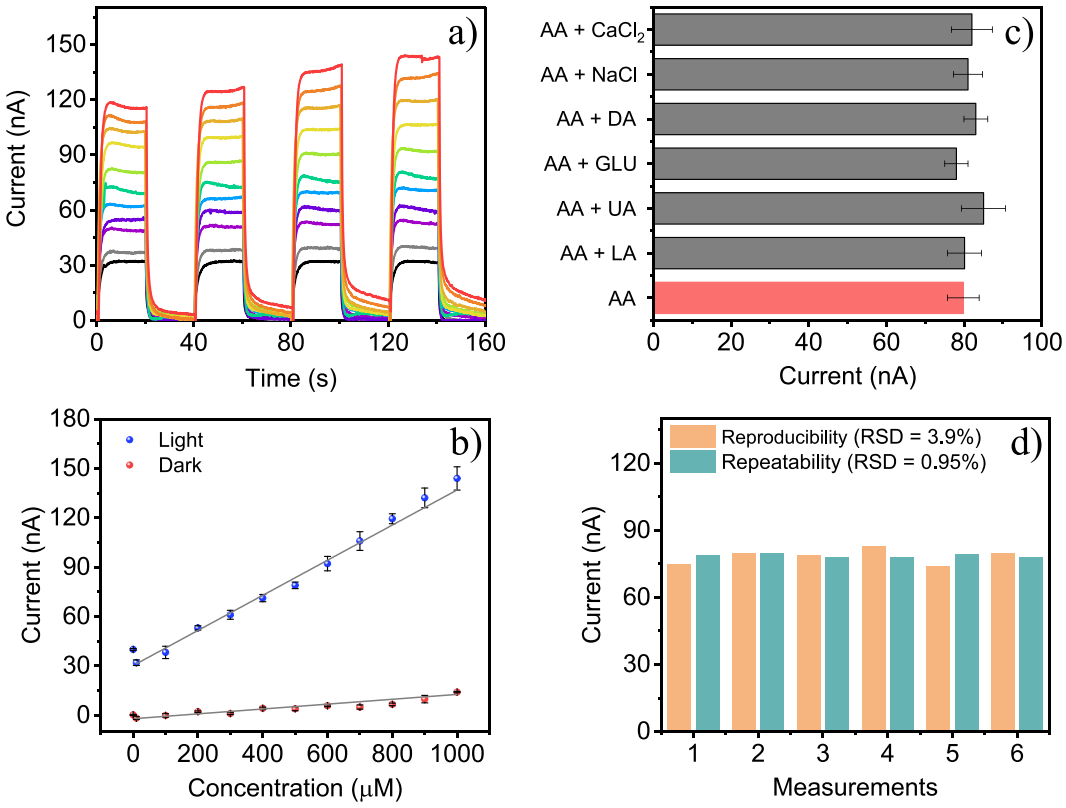

Fig. 5. (a) Transient photocurrent curves (10 – 1000 μM AA) and (b) analytical curve (blank, 10, 100, 200, 300, 400, 500, 600, 700, 800, 900 1000 μM AA) of TiO_2 recorded in 0.1 M PBS (n = 4). (c) Interference study with 500 μM AA and 1 mM Lactate (LA), uric acid (UA), glucose (GLU), dopamine (DA), NaCl, and $CaCl_2$. (d) Reproducibility and repeatability studies were obtained with 500 μM AA (n = 4). All photoelectrochemical experiments were recorded at 0 V vs. OCP under visible LED light irradiation (410 nm, 350 mW cm^{-2}).

Table 1
Performance comparison with other publications on AA detection.

Modification materials	Type	Linear range (μM)	LOD (μM)	Reference
CdS quantum dots	FC	0.06–0.3	0.002[a]	[32]
B, N, S *co*-doped carbon dots/Fe^{3+}	FC	0.1–600	0.05[a]	[33]
rGO/Fe_3O_4/GC	EC	10–100	18.52[a]	[34]
Graphene nanosheets/GC	EC	400–6000	120[a]	[35]
Fe_3O_4-SnO_2-graphene/GC	EC	0.1–23	0.063[a]	[36]
TiO_2-rGO	EC	25–725	1.19[b]	[37]
g-C_3N_4 nanosheets/GC	PEC	0.25–100	0.12[b]	[38]
$BiVO_4$/FTO	PEC	5–300	1[b]	[39]
TiO_2-10/SPCE	PEC	10–1000	3.25[b]	This work

[FC] Fluorescent.
[EC] Electrochemical.
[PEC] Photoelectrochemical.
[FTO] Fluorine doped tin oxide.
[SCPE] Printed Carbon Electrode.
[GC] glassy carbon.
[a] LOD calculated based $3S_b/m$, where S_b is the standard deviation of the blank signal and m is the slope of the linear range.
[b] LOD calculated based S/N = 3.

Data availability

No data was used for the research described in the article.

Acknowledgments

The authors are grateful for the financial support from the Brazilian agencies: São Paulo Research Foundation (FAPESP, grants 2018/22214-6, 2019/13514-9, 2022/00243-0 and 2022/03758-0).

Appendix A. Supplementary material

(F**igure S1) Equivalent circuit model; (Fi**gure S2) Raman spectra TiO_2 electrodeposited; (Fi**gure S3) SEM images of TiO_2 electrodeposited at 1000 times magnification; (Fi**gure S4) Cross-section SEM image of TiO_2-10 electrode in different regions; (Fi**gure S5) EDS analysis in cross-section of TiO_2-10 electrode; (Tab**le S1) D-spacing for TiO_2; (Tab**le S2) Recovery of AA.

Supplementary data to this article can be found online at https://doi.org/10.1016/j.apsusc.2023.158316.

References

[1] J.L. Bott-Neto, T.S. Martins, S.A.S. Machado, O.N. Oliveira Jr, Enhanced photocatalysis on graphitic carbon nitride sensitized with gold nanoparticles for photoelectrochemical immunosensors, Appl. Surf. Sci. 606 (2022), 154952, https://doi.org/10.1016/j.apsusc.2022.154952.
[2] T.S. Martins, J.L. Bott-Neto, O.N. Oliveira Jr, S.A.S. Machado, Paper-based electrochemical sensors with reduced graphene nanoribbons for simultaneous detection of sulfamethoxazole and trimethoprim in water samples, J. Electroanal. Chem. 882 (2021), 114985, https://doi.org/10.1016/j.jelechem.2021.114985.
[3] T.S. Martins, S.A.S. Machado, O.N. Oliveira Jr, J.L. Bott-Neto, Optimized paper-based electrochemical sensors treated in acidic media to detect carbendazim on the skin of apple and cabbage, Food Chem. 410 (2023), 135429, https://doi.org/10.1016/j.foodchem.2023.135429.
[4] J. Gañán, G. Martínez-García, S. Morante-Zarcero, D. Pérez-Quintanilla, I. Sierra, Nanomaterials-modified electrochemical sensors for sensitive determination of alkaloids: Recent trends in the application to biological, pharmaceutical and agri-food samples, Microchem. J. 184 (2023), 108136, https://doi.org/10.1016/j.microc.2022.108136.
[5] I.M. Mostafa, Y. Tian, S. Anjum, S. Hanif, M. Hosseini, B. Lou, G. Xu, Comprehensive review on the electrochemical biosensors of different breast cancer biomarkers, Sensors Actuators B Chem. 365 (2022), 131944, https://doi.org/10.1016/j.snb.2022.13194.

[6] S.F. Blaskievicz, L. Helena, Y. Zhao, F. Marken, Trends in Analytical Chemistry Semiconductor photoelectroanalysis and photobioelectroanalysis : A perspective, Trends Anal. Chem. 135 (2021), 116154, https://doi.org/10.1016/j.trac.2020.116154.

[7] D. Li, C. Batchelor-McAuley, L. Chen, R.G. Compton, Band Electrodes in Sensing Applications: Response Characteristics and Band Fabrication Methods, ACS Sensors. 4 (2019) 2250, https://doi.org/10.1021/acssensors.9b01172.

[8] M.S. Sumitha, T.S. Xavier, Recent advances in electrochemical biosensors – A brief review, Hybrid Adv. 2 (2023), 100023, https://doi.org/10.1016/j.hybadv.2023.100023.

[9] Z. Li, J. Zhang, Y. Huang, J. Zhai, G. Liao, Z. Wang, C. Ning, Development of electroactive materials-based immunosensor towards early-stage cancer detection, Coord. Chem. Rev. 471 (2022), 214723, https://doi.org/10.1016/j.ccr.2022.214723.

[10] A. Barhoum, S. Hamimed, H. Slimi, A. Othmani, F.M. Abdel-Haleem, M. Bechelany, Modern designs of electrochemical sensor platforms for environmental analyses: Principles, nanofabrication opportunities, and challenges, Trends Environ. Anal. Chem. 38 (2023) e00199.

[11] B. Wang, J.-T. Cao, Y.-M. Liu, Recent progress of heterostructure-based photoelectrodes in photoelectrochemical biosensing: a mini review, Analyst. 145 (2020) 1121, https://doi.org/10.1039/C9AN02448D.

[12] J. Shi, Z. Chen, C. Zhao, M. Shen, H. Li, S. Zhang, Z. Zhang, Photoelectrochemical biosensing platforms for tumor marker detection, Coord. Chem. Rev. 469 (2022), 214675, https://doi.org/10.1016/j.ccr.2022.214675.

[13] B. Bastug Azer, A. Gulsaran, J.R. Pennings, R. Saritas, S. Kocer, J.L. Bennett, Y. Devdas Abhang, M.A. Pope, E. Abdel-Rahman, M. Yavuz, A Review: TiO2 based photoelectrocatalytic chemical oxygen demand sensors and their usage in industrial applications, J. Electroanal. Chem. 918 (2022), 116466, https://doi.org/10.1016/j.jelechem.2022.116466.

[14] J.L. Bott-Neto, T.S. Martins, L.A. Buscaglia, P.V.B. Santiago, P.S. Fernández, S.A. S. Machado, O.N. Oliveira Jr., A portable system for photoelectrochemical detection of lactate on TiO_2 nanoparticles and [Ni(salen)] polymeric film, Sensors Actuators B Chem. 345 (2021), 130390, https://doi.org/10.1016/j.snb.2021.130390.

[15] J.L. Bott-Neto, T.S. Martins, L.A. Buscaglia, S.A.S. Machado, O.N. Oliveira, Photocatalysis of TiO_2 Sensitized with Graphitic Carbon Nitride and Electrodeposited Aryl Diazonium on Screen-Printed Electrodes to Detect Prostate Specific Antigen under Visible Light, ACS Appl. Mater. Interfaces. 14 (2022) 22114, https://doi.org/10.1021/acsami.2c03106.

[16] D. Dambournet, I. Belharouak, K. Amine, Tailored Preparation Methods of TiO_2 Anatase, Rutile, Brookite: Mechanism of Formation and Electrochemical Properties, Chem. Mater. 22 (2010) 1173, https://doi.org/10.1021/cm902613h.

[17] K. Priyalakshmi Devi, P. Goswami, H. Chaturvedi, Fabrication of nanocrystalline TiO2 thin films using Sol-Gel spin coating technology and investigation of its structural, morphology and optical characteristics, Appl. Surf. Sci. 591 (2022), 153226, https://doi.org/10.1016/j.apsusc.2022.153226.

[18] G. Žerjav, K. Žižek, J. Zavašnik, A. Pintar, Brookite vs. rutile vs. anatase: What's behind their various photocatalytic activities? J. Environ Chem. Eng. 10 (2022), 107722 https://doi.org/10.1016/j.jece.2022.107722.

[19] A.M. Alotaibi, S. Sathasivam, B.A.D. Williamson, A. Kafizas, C. Sotelo-Vazquez, A. Taylor, D.O. Scanlon, I.P. Parkin, Chemical Vapor Deposition of Photocatalytically Active Pure Brookite TiO_2 Thin Films, Chem. Mater. 30 (2018) 1353, https://doi.org/10.1021/acs.chemmater.7b04944.

[20] M. Machida, M. Kobayashi, Y. Suzuki, H. Abe, Facile synthesis of > 99% phase-pure brookite TiO_2 by hydrothermal conversion from Mg2TiO4, Ceram. Int. 44 (2018) 17562, https://doi.org/10.1016/j.ceramint.2018.06.170.

[21] P. Kanagavalli, C. Andrew, M. Veerapandian, M. Jayakumar, In-situ redox-active hybrid graphene platform for label-free electrochemical biosensor: Insights from electrodeposition and electroless deposition, TrAC Trends Anal. Chem. 143 (2021), 116413, https://doi.org/10.1016/j.trac.2021.116413.

[22] E.J. Choi, N.P. Drago, N.J. Humphrey, J. Van Houten, J. Ahn, J. Lee, I.-D. Kim, A. F. Ogata, R.M. Penner, Electrodeposition-enabled, electrically-transduced sensors and biosensors, Mater. Today. 62 (2023) 129, https://doi.org/10.1016/j.mattod.2022.11.021.

[23] C.D. Lokhande, B.-O. Park, H.-S. Park, K.-D. Jung, O.-S. Joo, Electrodeposition of TiO_2 and RuO_2 thin films for morphology-dependent applications, Ultramicroscopy. 105 (2005) 267, https://doi.org/10.1016/j.ultramic.2005.06.048.

[24] B. Endrődi, E. Kecsenovity, K. Rajeshwar, C. Janáky, One-Step Electrodeposition of Nanocrystalline TiO_2 Films with Enhanced Photoelectrochemical Performance and Charge Storage, ACS Appl. Energy Mater. 1 (2018) 851, https://doi.org/10.1021/acsaem.7b00289.

[25] J.N. Miller, J.C. Miller, Statistics and Chemometrics for Analytical Chemistry, Sixth Edit, 2010.

[26] D. Eisenberg, H.S. Ahn, A.J. Bard, Enhanced photoelectrochemical water oxidation on bismuth vanadate by electrodeposition of amorphous titanium dioxide, J. Am. Chem. Soc. 136 (2014) 14011, https://doi.org/10.1021/ja5082475.

[27] L.A. García-Contreras, J.O. Flores-Flores, J.Á. Arenas-Alatorre, J.Á. Chávez-Carvayar, Synthesis, characterization and study of the structural change of nanobelts of TiO_2 ($H_2Ti_3O_7$) to nanobelts with anatase, brookite and rutile phases, J. Alloys Compd. 923 (2022), 166236, https://doi.org/10.1016/j.jallcom.2022.166236.

[28] M. Choi, J. Lim, M. Baek, W. Choi, W. Kim, K. Yong, Investigating the Unrevealed Photocatalytic Activity and Stability of Nanostructured Brookite TiO_2 Film as an Environmental Photocatalyst, ACS Appl. Mater. Interfaces. 9 (2017) 16252, https://doi.org/10.1021/acsami.7b03481.

[29] Y. Ohno, K. Tomita, Y. Komatsubara, T. Taniguchi, K. Katsumata, N. Matsushita, T. Kogure, K. Okada, Pseudo-Cube Shaped Brookite (TiO_2) Nanocrystals Synthesized by an Oleate-Modified Hydrothermal Growth Method, Cryst. Growth Des. 11 (2011) 4831, https://doi.org/10.1021/cg2006265.

[30] O. Frank, M. Zukalova, B. Laskova, J. Kürti, J. Koltai, L. Kavan, Raman spectra of titanium dioxide (anatase, rutile) with identified oxygen isotopes (16, 17, 18), Phys. Chem. Chem. Phys. 14 (2012) 14567, https://doi.org/10.1039/c2cp42763j.

[31] S. Pigeot-Rémy, D. Gregori, R. Hazime, A. Hérissan, C. Guillard, C. Ferronato, S. Cassaignon, C. Colbeau-Justin, O. Durupthy, Size and shape effect on the photocatalytic efficiency of TiO2 brookite, J. Mater. Sci. 54 (2019) 1213, https://doi.org/10.1007/s10853-018-2924-x.

[32] M. Ganiga, J. Cyriac, An ascorbic acid sensor based on cadmium sulphide quantum dots, Anal. Bioanal. Chem. 408 (2016) 3699, https://doi.org/10.1007/s00216-016-9454-7.

[33] Y. Liu, Z. Wei, W. Duan, C. Ren, J. Wu, D. Liu, H. Chen, A dual-mode sensor for colorimetric and "turn-on" fluorescent detection of ascorbic acid, Dye. Pigment. 149 (2018) 491, https://doi.org/10.1016/j.dyepig.2017.10.039.

[34] J.S. Niranjana, H. Koyakutty, A.A. Thomas, M.J. Bushiri, Novel synthesis of multi-layered rGO/Fe_3O_4 nanocomposite in a single step and its efficient electrochemical sensing of vitamin C, Mater. Sci. Eng. B. 290 (2023), 116283, https://doi.org/10.1016/j.mseb.2023.116283.

[35] G.P. Keeley, A. O'Neill, N. McEvoy, N. Peltekis, J.N. Coleman, G.S. Duesberg, Electrochemical ascorbic acid sensor based on DMF-exfoliated graphene, J. Mater. Chem. 20 (2010) 7864, https://doi.org/10.1039/c0jm01527j.

[36] H. Bagheri, N. Pajooheshpour, B. Jamali, S. Amidi, A. Hajian, H. Khoshsafar, A novel electrochemical platform for sensitive and simultaneous determination of dopamine, uric acid and ascorbic acid based on Fe3O4SnO2Gr ternary nanocomposite, Microchem. J. 131 (2017) 120, https://doi.org/10.1016/j.microc.2016.12.006.

[37] F.A. Harraz, M. Faisal, A.A. Ismail, S.A. Al-Sayari, A.E. Al-Salami, A. Al-Hajry, M. S. Al-Assiri, TiO_2/reduced graphene oxide nanocomposite as efficient ascorbic acid amperometric sensor, J. Electroanal. Chem. 832 (2019) 225, https://doi.org/10.1016/j.jelechem.2018.11.004.

[38] R. Motaghed Mazhabi, L. Ge, H. Jiang, X. Wang, A facile photoelectrochemical sensor for high sensitive ROS and AA detection based on graphitic carbon nitride nanosheets, Biosens. Bioelectron. 107 (2018) 54, https://doi.org/10.1016/j.bios.2018.02.008.

[39] L. Li, M. Li, H. Liu, B. Li, B. Wang, A portable non-enzyme photoelectrochemical ascorbic acid sensor based on $BiVO_4$ electrode under 20 W LED light, J. Electroanal. Chem. 855 (2019), 113573, https://doi.org/10.1016/j.jelechem.2019.113573.

[40] D. Liu, Y. Qian, R. Xu, Y. Zhang, X. Ren, H. Ma, Q. Wei, A dual-signal amplification photoelectrochemical immunosensor for ultrasensitive detection of CYFRA 21–1 based on the synergistic effect of SnS_2/SnS/Bi_2S_3 and ZnCdS@NPC-ZnO, Sensors Actuators, B Chem. 346 (2021), 130456, https://doi.org/10.1016/j.snb.2021.130456.

[41] X.P. Liu, N. Chang, J.S. Chen, C.J. Mao, B.K. Jin, Ultrasensitive photoelectrochemical immunosensor based on a g-C_3N_4/SnS_2 nanocomposite for prostate-specific antigen detection, Microchem. J. 168 (2021), 106337, https://doi.org/10.1016/j.microc.2021.106337.

[42] Y. Zhou, Y. Wang, S. Li, X. Fang, H. Yin, P. Wang, S. Ai, A novel photoelectrochemical immunosensor for N1-methyladenine detection based on $BiVO_4$/g-C_3N_4 heterojunction with signal amplification of TiO_2@NH_2-MIL-125(Ti), Sensors Actuators, B Chem. 318 (2020), 128310, https://doi.org/10.1016/j.snb.2020.128310.